Available online at www.sciencedirect.com
SCIENCE DIRECT®
PERGAMON
International Journal of Heat and Mass Transfer 46 (2003) 4169–4177
International Journal of HEAT and MASS TRANSFER
www.elsevier.com/locate/ijhmt

Visualization of two-phase flow through microgrooved tubes for understanding enhanced heat transfer

Timothy A. Shedd [a,*], Ty A. Newell [b]

[a] Department of Mechanical Engineering, University of Wisconsin-Madison, 1500 Engineering Drive, Madison, WI 53706, USA

[b] Department of Mechanical and Industrial Engineering, University of Illinois at Urbana-Champaign, 1206 W. Green Street, Urbana, IL 61801, USA

Received 12 September 2001; received in revised form 28 April 2003

Abstract

Though widely used, questions remain as to the mechanisms by which micro-fin or microgrooved tubes enhance heat transfer performance. In this work, new experimental liquid film thickness profiles in adiabatic, air–water flow through clear tubes with 20 microgrooves at three different helix angles are presented. These results correlate well with the asymmetrical temperature measurements and heat transfer coefficients seen by previous investigators. Important observations include increased wall wetting for a given flow condition, decreasing influence of the grooves with increasing gas velocity, and a rotational redistribution of the liquid film by helical grooves, though without indication of a swirling behavior.

1. Introduction

Microgrooved (also called micro-fin) tubes play a very significant role in modern, high-efficiency refrigeration and air-conditioning systems. These tubes generally have grooves approximately 0.2 mm deep with about a 0.5 mm pitch which may be arranged in a variety of patterns around the inner walls. Currently, tubes with axial, helical, crosshatched and herringbone patterns are available. With their introduction about 20 years ago, it was found that microgrooved tubes demonstrate significantly increased heat transfer coefficients over smooth tubes with only a minor addition to pressure loss. This effect is most dramatic at low mass fluxes. Evidence from heat transfer data and flow visualization experiments indicate that the enhancement is due in large part to increased wetting of the tube perimeter, and various theories have been advanced to explain this. In this work, a non-intrusive, optical film thickness measurement system has been employed to document the liquid distribution in horizontal annular flow through tubes with axial and helical microgrooves. These results can be used to provide additional physical insight for the some of the mechanical behaviors underlying the heat transfer data reported in the literature.

2. Review of previous work

Substantial amounts of data have been gathered relating heat transfer behavior to system flow variables. Extensive reviews of pertinent heat transfer research in micro-fin tubes may be found in Newell and Shah [1] and Webb [2]. In what follows, investigations specifically related to the mechanics of liquid film distribution are discussed.

From the earliest studies of heat transfer in microgrooved tubes, tremendous enhancements in heat transfer coefficients were documented; much greater than could be accounted for by the increased surface area of the tube wall. Based on their heat transfer results and experimentation with the capillary rise of liquid up grooved flat plates, Ito and Kimura [3] and Kimura and Ito [4] suggested that capillary forces acting on liquid

* Corresponding author. Fax: +1-608-262-8464.
E-mail address: shedd@engr.wisc.edu (T.A. Shedd).

0017-9310/$ - see front matter © 2003 Elsevier Ltd. All rights reserved.
doi:10.1016/S0017-9310(03)00249-7

Nomenclature

d	diameter of the tube	G	mass flux (kg/m^2 s)
f	friction factor	$\dot{m}_g$	mass flow rate of vapor (kg/s)
Ft	Froude rate parameter, Eq. (1)	$\dot{m}_l$	mass flow rate of liquid (kg/s)
g	acceleration due to gravity	x	mass quality

refrigerant in the microgrooves was the dominant factor in the heat transfer enhancement they recorded. The importance of capillary forces is suggested by other researchers as well, including Cui et al. [5] and Yoshida et al. [6,7].

Experimental work of Khanpara et al. [8] and Schlager et al. [9] led these researchers to suggest that increased turbulence in the liquid film provides the mechanism for increased heat transfer. The decreased enhancement at higher mass fluxes is explained by the hypothesis that turbulence in the smooth tube film increases more rapidly with mass flux than in the finned tube.

The importance of flow pattern transitions, both accelerated and delayed, in the heat transfer behavior of enhanced tubes has been reported by more recent heat transfer research in both condensation and evaporation. Graham et al. [10] studied condensation in an axially finned tube and compared this with the condensation data of Ponchner and Chato [11] for an 18° helically finned tube. These data suggest that at low mass flux the helical grooves may be enhancing the drainage of condensate from the top of the tube to the bottom, allowing more of the tube wall surface area to be available for heat transfer. The axial fins, however, may inhibit this drainage, decreasing condensation effectiveness. At higher mass flux, the helical tube flow appears to transition to annular flow somewhat sooner than a smooth tube, but otherwise tends to show only an enhancement approximately equal to the percentage increase in surface area. The axial tube, however, by comparison with smooth tube data, seems to establish an annular flow pattern at very low qualities and thus shows significant enhancement in this region of operation.

Other researchers have suggested that flow pattern transitions had dominant influences on their data as well. In condensation, Koyama et al. [12] inferred what appeared to be transitions from annular to stratified flow from their circumferential temperature data. Sight glass observations allowed Singh et al. [13] to correlate improved evaporation heat transfer with a transition to annular flow. A similar transition was postulated by Zürcher et al. [14] based on comparison of R134a and R407C flow boiling data.

Flow visualization by several researchers has provided additional insight. Two-phase air–water studies carried out in horizontal transparent tubes with helical wire inserts were reported by Weisman et al. [15]. These investigators mapped transitions between flow behaviors and found that the transition from separated (stratified or wavy) to annular flow occurred at much lower superficial liquid and vapor velocities than in a smooth tube. A subsequent study by the same authors showed qualitatively similar behavior using refrigerant, R-113 [16].

Yoshida et al. [7] used a boroscope to observe R-22 flow inside of microgrooved tubing. Liquid was observed in the grooves around the entire circumference at all mass flux conditions. Where the liquid was thicker than the groove depth, it appeared to flow axially over the tops of the grooves. The liquid flowing in the grooves appeared to flow "slowly and rather smoothly along the grooves." At a mass flux of 50 kg/m^2 s, the liquid at the top of the tube appeared stagnant, with liquid in the grooves along the sides showing some oscillation. At mass flux conditions greater than 200 kg/m^2 s, the flow appeared to be annular, and, for qualities less than 0.8, the liquid film was thicker than the groove depth and the flow was generally axial.

A similar visualization technique was employed by Nozu and Honda [17], with the addition of a view looking axially down the tube near the exit of the test section. Observations of R-11 flow appear to show wavy stratified flow at 80 kg/m^2 s, annular flow with significant droplet entrainment at 110 kg/m^2 s and nearly uniform annular flow with fins continually submerged for a wide range of vapor quality at 175 kg/m^2 s. There is some possible indication of swirling or rotated flow of waves passing over the grooves, but this cannot be confirmed from the images presented. The exit pictures show that liquid tends to pool slightly asymmetrically with respect to the vertical; i.e. the liquid at the bottom of the tubes in these images tends to exit shifted counter-clockwise, the direction of groove rotation, when viewed from the flow direction.

3. Experimental setup

3.1. Test sections

Three transparent test sections with 20 microgrooves were fabricated with 0 (axial), 9° and 18° helix angles.

The test sections were constructed of 0.8 m lengths of 15.1 mm I.D. clear PVC tubing that where pulled over a die with four orthogonal cutting points set to cut triangular grooves 0.2 mm deep and 0.5 mm wide at the top. A guide sleeve slotted with the appropriate helix angle was used to rotate the tube during the cutting. This process was manual and prone to some inconsistency; the resulting grooves were not perfectly spaced nor as smooth as production quality copper tubes, as can be seen in Fig. 1a and b. The groove openings varied between 0.4 and 0.8 mm. After completing the grooves, the ends of these short lengths were milled square and were joined flush using a modified clear PVC coupling adapter such that the grooves aligned as closely as possible. The total observable length was about 6 m including a 3 m smooth flow development section. Only 20 grooves (as opposed to 60 in commercial tube of about this diameter) were cut into each tube to allow space for visualization between the grooves.

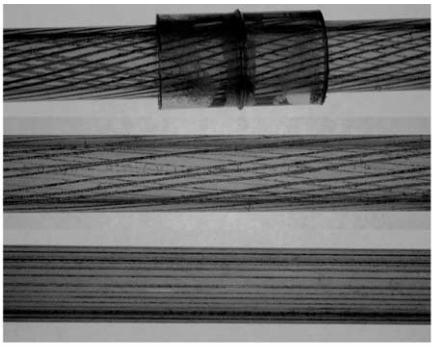

(a)

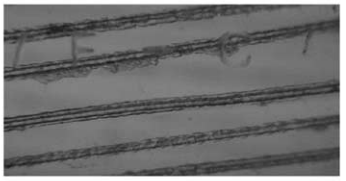

(b)

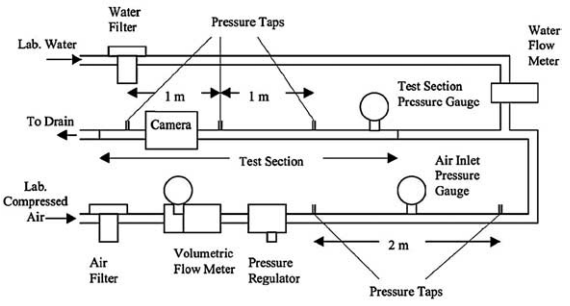

(c)

Fig. 1. (a) Photo of the grooved tubes used in this experiment, (b) magnified image of the grooves in the 9° tube (the width of the grooves is approximately 0.7 mm) and (c) experimental air/water test loop.

3.2. Flow loop

The primary experimental apparatus is shown in Fig. 1c. Laboratory compressed air was regulated and passed through a 3 m entrance tube. The mass flow rate of the air was determined by measuring the pressure drop across this entrance tube. The Colebrook correlation for friction factor, along with the definitions of friction factor, Reynolds number and mass flow rate, were then solved simultaneously to provide the mass flow rate of air in the loop. A propagation of error analysis performed for this experiment according to Taylor and Kuyatt [18] gives a total worst-case uncertainty of 3.5% in the air mass flow measurement. Comparison with an in-line spring-loaded volumetric flow meter using a compressed air source gave agreement to within the uncertainty of the flow meter. Water from the laboratory main passed through a bank of volumetric flow meters before entering the test section through several 1.6 mm holes drilled in the test section wall. Experimental uncertainties were ±5% based on manufacturer's data. Both the water and air were filtered to 5 μ prior to entering the apparatus.

Pressure gradients were measured using solid state differential pressure transducers. The inlet pressure transducer had a sensitivity of ±1.7 Pa while the test section transducers were sensitive to ±6.8 Pa. Gauge pressures in the entrance and test sections were monitored with Bourdon-tube gauges.

3.3. Film thickness measurement

Local liquid film thicknesses were obtained using an optical measurement system described in Shedd [19] and Shedd and Newell [20]. The time averaged liquid film thicknesses presented here were measured to within ±0.003 mm (±one standard error). Briefly, a point light source is placed on a transparent test section wall which has a translucent, diffusing coating on it. The light travels through the wall and liquid layer, but when it reaches the gas/liquid interface, any light arriving at an angle greater than or equal to the critical angle for the substances will be reflected back from the interface, creating a ring of light around the light source. The diameter of this light ring is directly proportional to the vertical distance traveled by the light. An image of this light ring is sampled at regular intervals and the mean liquid film thickness is determined from several hundred samples. If the surface is highly disturbed, the light will be significantly scattered and no measurement will be possible.

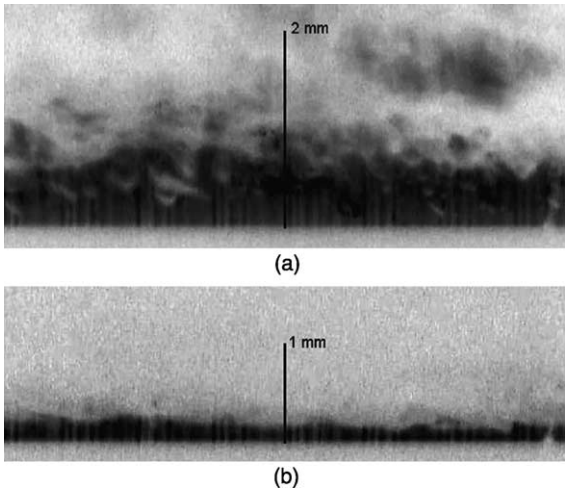

Fig. 2. (a) PLIF image of a wave in horizontal annular flow, (b) PLIF image of the film in between the waves under the same flow conditions.

Annular two-phase flow can be described as essentially composed of a thin liquid base film over which roll and disturbance waves flow. Images of the base film and a disturbance wave, obtained through planar laser induced fluorescence (PLIF), are shown in Fig. 2. As has been verified by Plzak and Shedd [21], the experimental results presented here exclude large liquid waves from the calculated average thickness; the thicknesses reported reflect only the thin base film that exists between the large liquid waves. This is significant since it is this thin base film that apparently plays the most active role in heat transfer [22]. Observations of annular flow indicate that, at a given instant, large waves cover less than 10% of the total tube length. The film thicknesses were measured at about 390 L/D from the point where liquid was introduced. The actual grooved length of each test section varied due to the nature of their fabrication. Film thickness was measured at 170 L/D, 140 L/D and 120 L/D from the beginning of the 0°, 9° and 18° grooved sections, respectively.

4. Experimental results

The flow conditions examined are shown in Table 1. The Froude rate is a non-dimensional group that essentially represents the ratio of the rate of kinetic energy flowing in the vapor to the power required to pump liquid from the bottom to the top of the tube at its axial flow rate. It is defined by

$$Ft = \left(\frac{\dot{m}_g}{\dot{m}_l}\right)^{0.5} Fr = \left(\frac{\dot{m}_g}{\dot{m}_l}\right)^{0.5} \left(\frac{U_{sg}}{(gd)^{0.5}}\right) \quad (1)$$

where the subscripts g and l represent vapor and liquid quantities, respectively, U_{sg} is the superficial vapor velocity (the velocity of vapor if it occupied the entire tube at the same mass flow rate), g is the gravitational acceleration and d is the tube diameter. Ft has been found to be a useful parameter for correlating some two-phase flow quantities [23,24]. In these calculations and those that follow, the nominal smooth diameter of the tube, 15.1 mm, is used.

4.1. Pressure drop

Fig. 3 plots the friction factors of the various tubes against the vapor Reynolds number. This plot reaffirms that the presence of grooves only generates a mild increase in pressure loss over smooth tubes in two-phase annular flow and has little effect on single-phase gas flow.

4.2. Film thickness

The liquid film thickness data at 16 circumferential locations for each of the seven flows are available in Shedd [25] for reference and direct comparison with other experimental and modeling results.

Liquid film thickness profiles for annular flow through the 0 (axial), 9° and 18° helix tubes are presented in Figs. 4–6. In each of these plots, the smooth tube profiles are shown by dotted lines while the grooved tube profiles are solid. The smooth tube profiles are essentially symmetrical left to right, but show the effects of

Table 1
Details of the experimental flow conditions

Name	$\dot{m}_g$ (kg/s)	$\dot{m}_l$ (kg/s)	Ft	x	G (kg/m^2 s)
T	0.0048	0.0032	70	0.6	44
U	0.0067	0.0032	120	0.68	55
V	0.0099	0.0032	210	0.76	73
Q	0.0047	0.0063	50	0.42	61
R	0.0079	0.0063	105	0.56	79
F	0.0110	0.0063	165	0.64	97
G	0.0152	0.0063	250	0.71	120

Ft is the Froude rate, x is quality and G is mass flux. See text for an explanation of the Froude rate parameter.

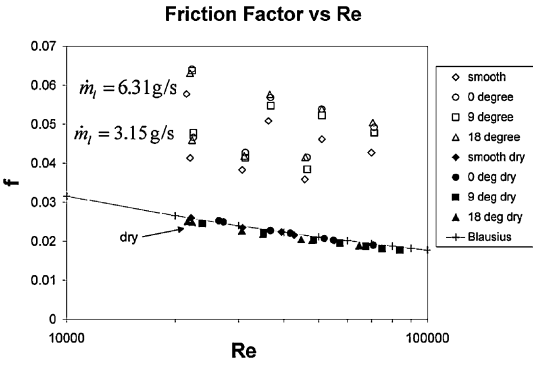

Fig. 3. Friction factor versus Reynolds number for various flow conditions in the four different tubes.

gravity with thicker liquid on the bottom. Contrast with these the profiles of the helically grooved tubes. First, the thickest parts of these films appears to have been rotated counterclockwise (the same direction as the groove helix), so that these films seem to be symmetrical about a line passing through the center of the tube at some angle from upper left to lower right. Second, the amount of wetted tube periphery is substantially increased. In the lowest flow approximately 62% of the smooth tube is wetted versus 81% of the 9° and 94% of the 18° tubes. The profiles of the 9° and 18° tubes seem quite similar to that which is found when liquid is placed inside a rotating cylinder. Or, in other words, it appears that a circumferential shear, due to the grooves, occurs at the wall.

It should be noted, however, that this rotation effect, if it exists, acts in combination with several other mechanisms to generate the steady profiles shown above. Tracking of small bubbles and particles in the film using a digital video camera and a high-speed strobe light gave no real indication of a rotation or swirling motion propagating into the bulk of the film layer. At low mass flux conditions, steady profiles would form with sections of the tube dried out. These dryout patches did not follow the grooves for long lengths. Typically, the film would dry out in a roughly rectangular region that was more or less horizontal, cutting across several grooves, rather than following the groove angle. If the film were swirling (having a helical trajectory), the dryout patches should follow some helical pattern, which was not observed. These dry patches were quite stable, lasting several minutes, and the overall dryout pattern was reproducible, indicating that the film was in some sort of mechanical equilibrium.

The 0°, or axially grooved, tube behaved differently than the other two. Most noticeable were the regions on the sides of the tube where a stable, thicker film appears to form. These may be indications that forces pushing liquid up the wall meet resistance in the groove; these

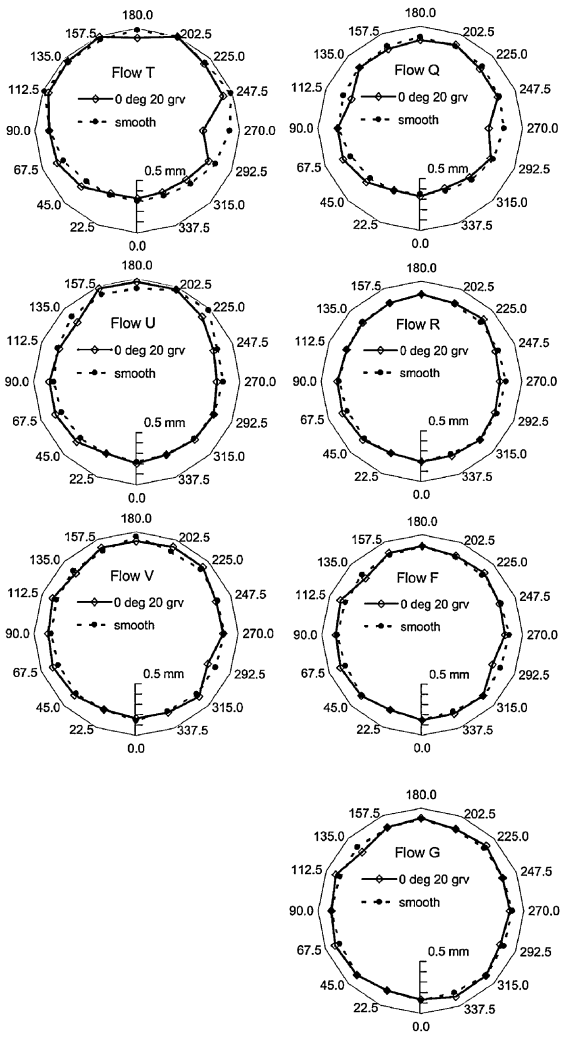

Fig. 4. Film thickness profiles in tube with 0° helix grooves compared with the smooth tube profiles with liquid flow of 0.003 kg/s (flows T, U and V) and 0.006 kg/s (flows Q, R, F and G).

locations may reflect the equilibrium reached between the upward forces and gravity in the presence of the horizontal grooves.

5. Discussion

There are significant differences between the test sections used in this study and the enhanced tubes used in commercial applications. Further differences exist between pure refrigerant flow and the two-phase flow of air and water. However, the film thickness data presented in this study agree well with the asymmetrical wall temperature and heat transfer coefficient measurements

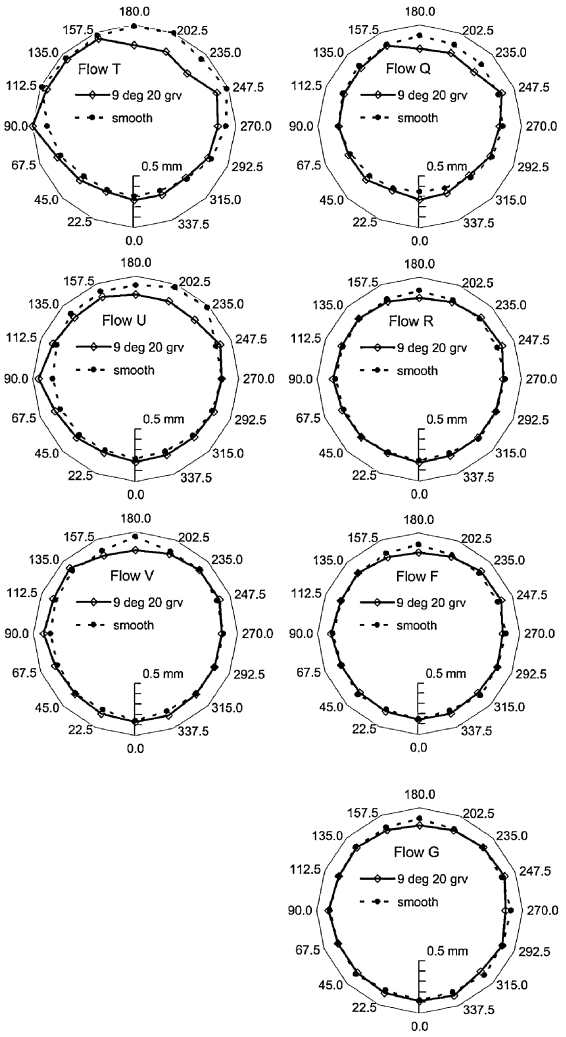

Fig. 5. Film thickness profiles in tube with 9° helix grooves compared with the smooth tube profiles with liquid flow of 0.003 kg/s (flows T, U and V) and 0.006 kg/s (flows Q, R, F and G).

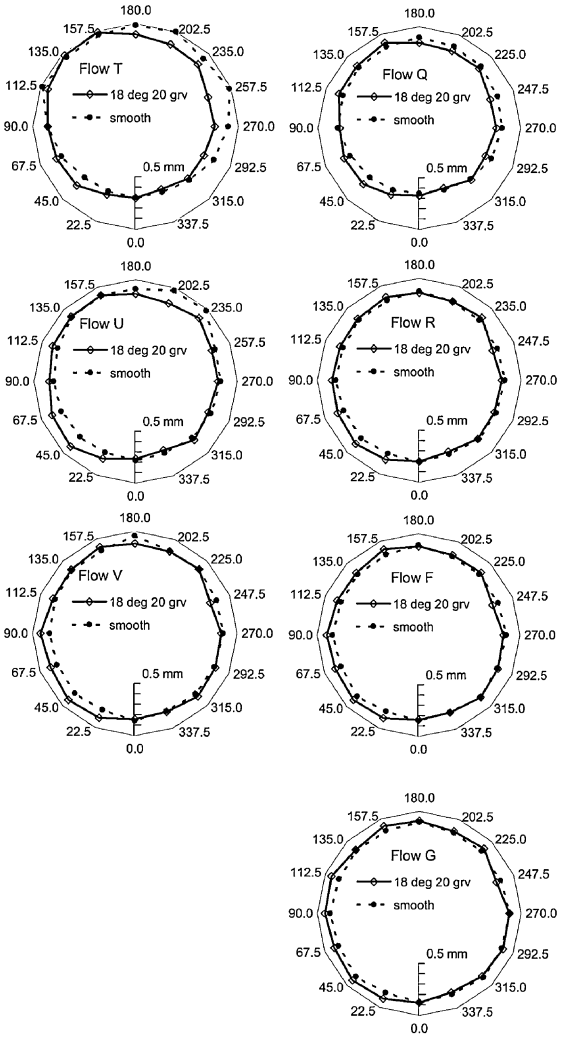

Fig. 6. Film thickness profiles in tube with 18° helix grooves compared with the smooth tube profiles with liquid flow of 0.003 kg/s (flows T, U and V) and 0.006 kg/s (flows Q, R, F and G).

that appear in several works, suggesting that the current experimental apparatus is able to capture important mechanical behaviors the exist in the commercial tubes. Recent work of Blankenberger and Shedd [26] and Rodriguez and Shedd [27] shows that horizontal air/water flows exhibit very similar pressure drop, film thickness and wave behavior as refrigerant flows with matching vapor (gas) kinetic energy. In addition, in annular flow, modeling efforts of DelCol et al. [28] found that surface tension and wetability effects were negligible for qualities below $x = 0.8$ due to the fact that the fin tips will be completely submerged, as experimentally documented by Yoshida et al. [7]. Thus, air/water annular flow through the current test sections should serve as a reasonable platform for investigating the mechanical behaviors that govern the heat transfer in commercial micro-fin tubes.

5.1. Asymmetrical wall temperature distributions

Yoshida et al. [6] present circumferential heat transfer coefficient data for evaporation at two mass flux conditions and over a quality range from 0.1 to 1. For R-22 at 100 kg/m^2 s, the heat transfer coefficient at the top of a smooth tube is very near zero, while it is very high (reaches 8 kW/m^2 K) at the top of the grooved tube. This indicates that the grooves are causing a thin film of refrigerant to form on the top of the grooved tube. These researchers do not measure both sides of the tube, but it is interesting that at low qualities, the heat transfer is

greatest at the one measured side for the smooth tube, which may be expected because of a thin meniscus at the edges of the stratified layer or a thin film left behind by waves. In the grooved tube, however, the data consistently show the right side value in between the bottom and top, and the heat transfer is generally much more uniform over the tube throughout the whole quality range. Heat transfer coefficients in the grooved tube tend to be three or four times that in the smooth tube at low mass flux (100–200 kg/m^2 s). At 300 kg/m^2 s, the heat transfer in the grooved tube is only about 1.3 times that in the smooth tube, and both sets of data indicate the flow is annular with a fairly uniform temperature distribution around the circumference of the tube. Very similar results have been described by Ebisu and Torikoshi [29], Koyama et al. [12], and Oh and Bergles [30] using a variety of refrigerants in both condensation and evaporation.

These studies bring out common behaviors in the circumferential measurements of heat transfer. First, at conditions where liquid flow in a smooth tube would be expected to be stratified with little heat transfer occurring through the top of the tube, the micro-fin tubes show very high heat transfer coefficients. Next, these heat transfer coefficients tend to be asymmetrical. The highest heat transfer takes place on the top or left side of the tube, the lowest to the bottom and right.

This behavior appears to be well described by the film thickness results obtained in this study. Looking at Figs. 5 and 6, it is apparent that the grooves act to distribute liquid counterclockwise, from the bottom to the top. The profiles are also asymmetrical, being thinnest in the upper left and thickest in the lower right. It appears, then, that the grooves are contributing to heat transfer enhancement by assisting in the transition from stratified to annular flow, and that detailed knowledge of the liquid film distribution can lead to accurate predictions of circumferential heat transfer coefficients.

5.2. The effects of mass flux

No clear explanation for the decrease in heat transfer enhancement with increase mass flux has been offered in the literature. The current experimental results offer insight. As can be seen from the plots of film profiles in Figs. 4–6, as mass flux and/or quality increases, the film profiles in the grooved tubes approach the profiles in the smooth tubes very closely. Based on this result, it can be said that the heat transfer enhancement at high quality and/or high mass flux is due almost solely to the increased surface area offered by the grooves.

5.3. Condensation versus evaporation

In most commercial applications, condensation takes place at higher saturation temperatures and pressures than evaporation. Vapor densities at these conditions are frequently about three times greater than those at typical evaporation conditions. At the same mass flux, then, vapor velocities are lower. This impacts heat transfer in multiple ways. For example, slower vapor has less energy to distribute liquid around the tube walls, creating less uniform liquid distributions. Pressure losses will also be lower per unit length. This is emphasized by the work of Yashar et al. [24] who found that void fraction shows a dependence on mass flux in their lower mass flux condensation data compared with evaporation data at the same flow conditions. Apparently, the refrigerant flow in condensation indicated a transition from dominantly stratified to primarily annular flow as mass flux increased, while the evaporating refrigerant (at lower pressures) remained annular through all mass flux conditions.

Evidence of the impact of flow behavior on heat transfer is also shown by the studies of Schlager et al. and Eckels et al. Schlager et al. [9] found that, using R22, enhancement factors were greater for evaporation than for condensation, especially at the lowest mass flux conditions (125 kg/m^2 s). The differences in enhancement factors decreased as a mass flux of 400 kg/m^2 s was approached. Zürcher et al. [31] noted from their evaporation data that while the micro-fin tube had appeared to force R134a into annular flow, at the same temperatures, R407C, operating at almost twice the pressure, appeared to remain in a wavy stratified flow. This is also partially supported by condensation data provided by Fujii [32] who compared enhancement factors of R22, R134a and R123. As working pressure increased with these fluids, the enhancement became less dependent on mass flux.

The data obtained in this work show the effect of vapor velocity on liquid film distribution as can be seen in the flow images of Figs. 5 and 6. At the lowest air velocity, significant asymmetry exists in the liquid film thickness, though the grooved tubes show more even film distribution than the smooth tubes. As air velocity increases, so does the symmetry of the liquid.

5.4. Correlation of peaks in heat transfer and pressure drop

Studies performed by Nidegger et al. [33], and Zürcher et al. [14,31,34] for evaporation of R134a and R407C in smooth and micro-fin tubes indicate a strong correlation between heat transfer data and pressure drop data, particularly at high qualities. As quality increases, heat transfer coefficients peak at qualities ranging from 0.75 to 0.95, depending on the mass flux; the pressure drop data show very similar peaks.

The peaks in both heat transfer and pressure drop mark the onset of dryout in the tube. This form of dryout is discussed in Shedd [25] and is apparently

caused by vapor shearing the liquid layer to a point where the liquid can no longer maintain continuity. Just prior to this point, the film will be at its thinnest and most uniform distribution, leading to the lowest heat transfer resistance for that flow condition. In addition, the accelerational pressure drop will be greatest due to high velocity vapor interacting with a continuous liquid layer. Once dryout begins, heat transfer immediately falls. Pressure drop decreases as well because the dry wall, whether smooth or grooved, offers much less flow resistance than the liquid film.

6. Conclusion

Using the results of detailed film thickness measurements, a more complete picture of the mechanisms of heat transfer augmentation in enhanced tubes has been presented. These results show that helical grooves promote earlier transitions to annular flow and give a rotated asymmetrical liquid film profile. These liquid profiles correspond to circumferential heat transfer measurements reported in the literature. In addition, the increased uniformity of the film at high qualities provides an explanation for the decrease in enhancement at higher mass flux and/or qualities seen in the literature.

Significant issues remain as to how exactly the grooves affect the liquid film. The effect of groove angle and the number of grooves on heat transfer is not clear. In addition, it will be important to quantify the forces acting on the liquid film in grooved tubes so that accurate models of heat transfer and pressure drop can be built. Finally, more investigation needs to be done before the unique behavior of the axially grooved tubes can be understood.

Acknowledgements

This work was supported by the Air Conditioning and Refrigeration Center at the University of Illinois at Urbana-Champaign, an NSF Industry-University Cooperative Research Center. Thanks to undergraduate research assistant Robert Shurig for his help in obtaining much of the film thickness data.

References

[1] T.A. Newell, R.K. Shah, An assessment of refrigerant heat transfer, pressure drop, and void fraction effects in microfin tubes, HVAC&R Res. 7 (2) (2001) 125–153.

[2] R.L. Webb, Principles of Enhanced Heat Transfer, John Wiley & Sons, Inc., New York, 1990.

[3] M. Ito, H. Kimura, Boiling heat transfer and pressure drop in internal spiral-grooved tubes, Bull. JSME 22 (171) (1979) 1251–1257.

[4] H. Kimura, M. Ito, Evaporating heat transfer in horizontal internal spiral-grooved tubes in the region of low flow rates, Bull. JSME 24 (195) (1981) 1602–1607.

[5] S. Cui, Y. Tan, Y. Lu, Heat transfer and flow resistance of R-502 flow boiling inside horizontal ISF tubes, in: X.-J. Chen, T.N. Veziroğlu, C.L. Tien (Eds.), Multiphase Flow and Heat Transfer: Second International Symposium, vol. 1, Hemisphere Publishing Corp., 1992, pp. 662–670.

[6] S. Yoshida, T. Matsunaga, H.P. Hong, K. Nishikawa, Heat transfer to refrigerants in horizontal evaporator tubes with internal, spiral grooves, in: P.J. Marto (Ed.), Proceedings of the 1987 ASME–JSME Thermal Engineering Joint Conference, vol. 5, 1987, pp. 165–172.

[7] S. Yoshida, T. Matsunaga, H.P. Hong, K. Nishikawa, Heat transfer enhancement in horizontal, spirally grooved evaporator tubes, JSME Int. J. 31 (3) (1988) 505–512.

[8] J.C. Khanpara, M.B. Pate, A.E. Bergles, Local evaporation heat transfer in a smooth tube and a micro-fin tube using refrigerants 22 and 113, in: Boiling and Condensation in Heat Transfer Equipment. Presented at the Winter Annual Meeting of the American Society of Mechanical Engineers, vol. HTD-85, ASME, Boston, MA, 1988, pp. 31–39.

[9] L.M. Schlager, M.B. Pate, A.E. Bergles, Evaporation and condensation heat transfer and pressure drop in horizontal, 12.7-mm microfin tubes with refrigerant 22, J. Heat Transfer—Trans. ASME 112 (1990) 1041–1047.

[10] D. Graham, J.C. Chato, T.A. Newell, Heat transfer and pressure drop during condensation of Refrigerant 134a in an axially grooved tube, Int. J. Heat Mass Transfer 42 (11) (1999) 1935–1944.

[11] M. Ponchner, J.C. Chato, Condensation of HFC-134a in an 18° helix angle micro-finned tube, Tech. Rep. TR-75, Air Conditioning and Refrigeration Center, University of Illinois at Urbana-Champaign, Urbana, IL, 1995.

[12] S. Koyama, A. Miyara, H. Takamatsu, T. Fujii, Condensation heat transfer of binary refrigerant mixtures of R22 and R114 inside a horizontal tube with internal spiral grooves, Int. J. Refrig. 13 (1990) 256–263.

[13] A. Singh, M.M. Ohadi, S. Dessiatoun, Flow boiling heat transfer coefficients of R-134a in a microfin tube, J. Heat Transfer—Trans. ASME 118 (1996) 497–499.

[14] O. Zürcher, J.R. Thome, D. Favrat, In-tube flow boiling of R-407C and R-407C/oil mixtures. Part II: Plain tube results and predictions, HVAC&R Res. 4 (4) (1998) 373–399.

[15] J. Weisman, J. Lan, P. Disimile, Two-phase (air–water) flow patterns and pressure drop in the presence of helical wire ribs, Int. J. Multiphase Flow 20 (5) (1994) 885–899.

[16] J. Weisman, J. Lan, P. Disimile, The effect of fluid properties on two-phase (vapor–liquid) flow patterns in the presence of helical wire ribs, Int. J. Multiphase Flow 22 (3) (1996) 613–619.

[17] S. Nozu, H. Honda, Flow characteristics of condensing two-phase flow in horizontal microfin tubes, ASME Fluids Eng. Div. 244 (1997) 119–130.

[18] B.N. Taylor, C.E. Kuyatt, Guidelines for evaluating and expressing uncertainty of NIST measurement results, Tech. Rep. 1297, National Institute of Standards and Technology, Bethesda, MD, 1994.

[19] T.A. Shedd, An automated optical liquid film thickness measurement method, Master's Thesis, University of Illinois at Urbana-Champaign, Urbana, IL, 1998.

[20] T.A. Shedd, T.A. Newell, Automated optical liquid film thickness measurement method, Rev. Sci. Instrum. 69 (12) (1998) 4205–4213.
[21] K.M. Plzak, T.A. Shedd, Verification of an optical liquid film thickness measurement system in horizontal annular two-phase flow, Exp. Fluids, submitted for publication.
[22] S. Jayanti, G.F. Hewitt, Hydrodynamics and heat transfer in wavy annular gas–liquid flow: a computational fluid dynamics study, Int. J. Heat Mass Transfer 40 (10) (1997) 2445–2460.
[23] E.T. Hurlburt, T.A. Newell, Prediction of the circumferential film thickness distribution in horizontal annular gas–liquid flow, J. Fluids Eng.—Trans. ASME 122 (2000) 1–7.
[24] D.A. Yashar, D.M. Graham, M.J. Wilson, J.C. Chato, H.R. Kopke, T.A. Newell, An investigation of refrigerant void fraction in horizontal, microfin tubes, HVAC&R Res. 7 (1) (2001) 67–82.
[25] T.A. Shedd, Characteristics of the liquid film in horizontal two-phase annular flow, Ph.D. Thesis, University of Illinois at Urbana-Champaign, Urbana, IL, 2001.
[26] P.L. Blankenberger, T.A. Shedd, Comparison of R-123 flow behavior to air/water flow behavior for horizontal flow, in: J. Klausner (Ed.), Proceedings of the 5th International Conference on Boiling Heat Transfer, Montego Bay, Jamaica, 2003.
[27] D.J. Rodriguez, T.A. Shedd, Study of potential enhancement of heat transfer by bubble entrainment in horizontal flow boiling, in: J. Klausner (Ed.), Proceedings of the 5th International Conference on Boiling Heat Transfer, Montego Bay, Jamaica, 2003.
[28] D. DelCol, R.L. Webb, R. Narayanamurthy, Heat transfer mechanisms for condensation and vaporization inside a microfin tube, J. Enhanced Heat Transfer 9 (1) (2002) 25–37.
[29] T. Ebisu, K. Torikoshi, Experimental study on evaporation and condensation heat transfer enhancement for R-407C using herringbone heat transfer tube, ASHRAE Trans. 106 (1998) 1044–1052.
[30] S.Y. Oh, A.E. Bergles, Visualization of the effects of spiral angle on the enhancement of in-tube flow boiling in microfin tubes, ASHRAE Trans. 108 (2) (2002) 509–515.
[31] O. Zürcher, J.R. Thome, D. Favrat, In-tube flow boiling of R-407C and R-407C/oil mixtures. Part I: Microfin tube, HVAC&R Res. 4 (4) (1998) 347–372.
[32] T. Fujii, Enhancement to condensing heat transfer, J. Enhanced Heat Transfer 2 (1–2) (1995) 127–137.
[33] E. Nidegger, J.R. Thome, D. Favrat, Flow boiling and pressure drop measurements for R-134a/oil mixtures. Part 1: Evaporation in a microfin tube, HVAC&R Res. 3 (1) (1997) 38–53.
[34] O. Zürcher, J.R. Thome, D. Favrat, Flow boiling and pressure drop measurements for R-134a/oil mixtures. Part 2: Evaporation in a plain tube, HVAC&R Res. 3 (1) (1997) 54–64.